Effect of the Volume Fraction on the Average Flocculation Rate

German Urbina-Villalba,* Jhoan Toro-Mendoza, Aileen Lozsán, and Máximo García-Sucre

Centro de Física, Laboratorio de Fisicoquímica de Coloides, Instituto Venezolano de Investigaciones Científicas (IVIC), Aptdo. 21827, Caracas 1020-A, Venezuela

Received: December 19, 2003; In Final Form: February 13, 2004

Brownian dynamics simulations are used to study the effect of the volume fraction of internal phase ($10^{-5} \leq \phi \leq 0.40$) on the flocculation rate (k_f) of oil in water (O/W) emulsions. To cover the typical range of Hamaker constants, its characteristic value for a bitumen emulsion ($A = 1.24 \times 10^{-19}$ J) and its typical order of magnitude for a latex dispersion ($A = 1.24 \times 10^{-21}$ J) were used. Account of hydrodynamic interactions was made, using a new methodology [Urbina-Villalba et al. *Phys. Rev. E* **2003**, *68*, 061408], which incorporates local volume fraction corrections at intermediate separations, and exact hydrodynamic interactions at closer distances. The resulting flocculation rates and their half-lifetimes ($t_{1/2}$) were analyzed as a function of the volume fraction and the initial mean free path (l) between the drops. Useful approximate relations are found for a limited range of volume fractions. Despite the fact that ϕ and l^{-2} are related and $t_{1/2}$ should decrease with either one, while k_f is expected to increase, the quality of the fittings was different, depending on the Hamaker constant and the variable chosen. For $A = 1.24 \times 10^{-21}$ J, the best correlation involves $t_{1/2}$ and ϕ. In the case of $A = 1.24 \times 10^{-19}$ J, the best fits contain k_f and either ϕ or l^{-2}. In general, the flocculation rate decreases monotonically as the volume fraction lowers, approaching the theoretical estimation. Values of k_f below the theoretical prediction, as those occasionally found in experimental evaluations of very dilute systems, were not observed.

Introduction

According to Smoluchowski's theory of coagulation,[1] the total number of particles per unit volume of a dispersion (n) decreases with time according to eq 1:

$$n = \frac{n_0}{1 + k_f n_0 t} \tag{1}$$

Here, n_0 is the initial particle density, t the time, and k_f the flocculation rate, which in the absence of interaction forces is equal to

$$k_f^{-1} = n_0 t_{1/2} = \frac{1}{8\pi a D_0} = \frac{3\eta}{4k_B T} \tag{2}$$

where k_B is the Boltzmann constant, and $t_{1/2}$ is the time required for the number of particles to drop to $n_0/2$. Its expression can be calculated substituting n by $n_0/2$ in eq 1. It is also clear from eq 1 that the product $k_f n_0$ is the frequency of collisions between particles. The inverse of this product has the dimension of time, and is equivalent to the mean time between collisions ($t_f = 1/k_f n_0$). Thus, the first equality in eq 2 illustrates the fact that the flocculation rate is inversely proportional to the average time between collisions t_f, which in turn is equal to $t_{1/2}$ ($t_f = t_{1/2}$). The last equality in eq 2 can be obtained substituting D_0 by the diffusion constant of a solid particle at infinite dilution:

$$D_0 = \frac{k_B T}{6\pi\eta\, a} \tag{3}$$

where a stands for the particle radius, and η refers to the viscosity of the surrounding medium.

The above equations were deduced imagining one of the particles to be stationary while all others collide with it due to their Brownian motion. The following assumptions were made: (a) every collision was effective; (b) the shape of the collision surface was approximately the same despite the flocculation of the central particles with other particles;[2] and (c) the relative diffusion constant between two particles was equal to the sum of their absolute diffusion constants. As a result of these assumptions, the theoretical expression for the flocculation rate between aggregates of different sizes (k_{ij}) comes out to be roughly the same:[3]

$$k_{ij} = \frac{kT}{3\eta}\frac{(a_i + a_j)^2}{a_i a_j} \approx k_f \tag{4}$$

The previous simplification, along with the assumption of irreversible flocculation, allowed Smoluchowski to establish the variation of the particle size distribution (PSD) as a function of time. Accordingly, the number of aggregates composed of "i" initial particles at time t was found to be equal to

$$n_i = \frac{n_0[k_f n_0 t]^{i-1}}{[1 + k_f n_0 t]^{i+1}} \tag{5}$$

Modifications of eq 1 regarding polydispersity[4−7] and the effect of repulsive barriers[8,9] are known. It is clear that this simple theory cannot account for complex effects such as drop deformation or surfactant diffusion, in which case, either simulations or more elaborate formalisms should be employed. Despite its shortcomings, Smoluchowski's theory had been very

* Author to whom correspondence should be addressed. E-mail: guv@ivic.ve.

10.1021/jp0313270 CCC: $27.50
Published on Web 04/06/2004

successful in describing the dynamics of aggregation of solid dispersions. In dilute systems, former experimental techniques (ultramicroscopy, Coulter counter, number fluctuation spectroscopy[3]) and more recently single-particle light scattering[10,11] nicely reproduce the form of the theoretical curves for the variation of the number of particles with time. Still, some discrepancies exist regarding the value of the flocculation rates for different particle sizes, k_{ij}, and the exact magnitude of k_f in the limit of very low volume fractions.[3] These deviations had been explained in terms of reversible flocculation, hydrodynamic interactions, and the presence of a repulsive barrier.[3,10] The effect of hydrodynamic interactions (HI) is also believed to be especially important at high concentrations, where the experimental quantification of the flocculation constant is very difficult.

In this article we study the dependence of the flocculation rate on the volume fraction of particles using Brownian dynamics simulations with proper account of HI. As will be shown, the results are compatible with the predictions of Smoluchowski theory for a limited but ample range of volume fractions if the flocculation constant is used as an adjustable parameter, sensibly dependent on the value of ϕ.

Hydrodynamic Interactions. Hydrodynamic effects enter the theory of aggregation through the value of the diffusion constant (eq 3) and by way of the assumption that the relative diffusion constant between two particles is equal to the sum of their individual contributions. The diffusion constant is clearly defined in those cases where the diffusion tensor is diagonal (for one symmetrical particle at infinite dilution). Even in this case, the specific form of the diffusion constant depends on the boundary conditions between the solvent media and the particle surface assumed for the solution of the Navier−Stokes equation. Equation 3 was calculated for the case of solid particles supposing a zero perpendicular velocity of the liquid at the particle surface. In the case of liquid drops or whenever the surface of the particles is modified by surfactant adsorption, the diffusion constant at infinite dilution already presents a different analytical form.[12−14] In such cases, the theoretical flocculation rate given by eq 2 may change due to the variation of D_0.

In a dispersion, an effective diffusion constant can be obtained by averaging mobility functions on particle configurations.[15−16] The mobility functions for a set of suspended particles are the coefficients of the total diffusion matrix of the system.[17−19] The elements of the diffusion matrix are equal to[12−14]

$$\mathbf{D}_{ii} = D_0\hat{I} + D_0 \sum_{j=1,j\neq i} \{A_s(r_{ij})\hat{r}_{ij}\hat{r}_{ij} + B_s(r_{ij})[\hat{I} - \hat{r}_{ij}\hat{r}_{ij}]\} \quad (6)$$

$$\mathbf{D}_{ij} = D_0\{A_c(r_{ij})\hat{r}_{ij}\hat{r}_{ij} + B_c(r_{ij})[\hat{I} - \hat{r}_{ij}\hat{r}_{ij}]\} \quad (7)$$

where, i and j are particle labels, $\hat{\mathbf{r}}_{ij} = \mathbf{r}_{ij}/r_{ij}$, $\mathbf{r}_{ij} = \mathbf{r}_i - \mathbf{r}_j$ is the distance between the particles, and $\mathbf{r}_i$ is the position vector of particle i. The summation in eq 6 indicates that the diffusion of a particle depends on the flux of liquid generated by its movement and reflected by the surrounding particles. Additionally, its diffusion is a function of the fluxes directly generated by their neighbors (eq 7) as they move.

The scalar functions A_s, B_s, A_c, and B_c in eqs 6 and 7 are the referred mobility functions. Their analytical expressions depend on the particle radii, and are usually evaluated supposing pairwise additive interactions.[17−19] As a consequence they overestimate the effect of hydrodynamic interactions (HI) in concentrated systems where screening occurs.[20−21]

Effective diffusion constants can be obtained from light scattering experiments,[22−24] or can be analytically deduced

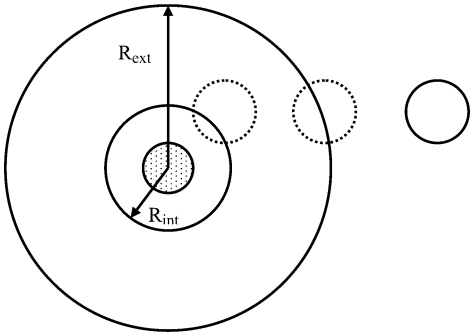

Figure 1. To calculate the effect of hydrodynamic interactions (HI) on the movement of a given particle, C, internal and external radii are defined. Particles beyond R_{ext}, do not influence the movement of C. Particles between R_{int} and R_{ext} contribute to the calculation of a local volume fraction ϕ. This allows the evaluation of $D(\phi,d)$ from eq 8 unless there is at least one particle within the internal radii ($r_{ij} \leq R_{int}$) previously defined. In this case, eqs 9−10 are used to calculate $D(\phi,d)$ employing the distance of closest approach to evaluate β (eqs 10).

averaging mobility functions over two- and three-particle distribution functions:[12,15−16]

$$D(\phi) = D_0(1 - 1.734\phi + 0.91\phi^2...) \quad (8)$$

Recently, a novel methodology for the calculation of an effective diffusion constant in concentrated systems[25] was proposed. It makes use of a local volume fraction correction of the diffusion constant (given by eq 8), along with a rational expression proposed by Honig et al.[26] for the case of two flocculating particles at close separation.[27] The referred methodology is illustrated in Figure 1. To calculate the HI of a central particle, its surrounding space is divided into three regions delimited by an internal (R_{int}) and an external (R_{ext}) radius. Particles in the outermost region $d > R_{ext}$ ($d = r_{ij} - a_i - a_j$) do not contribute to the HI of the central particle. Particles in the intermediate region ($R_{int} < d \leq R_{ext}$) contribute with the fraction of their volume inside that region to the calculation of a local volume fraction around the central particle. Once the local volume fraction has been evaluated, eq 8 can be used for the computation of an effective diffusion constant $D(\phi,d)$. Whenever a particle is located within the internal region ($d \leq R_{int}$), the value of the local volume fraction is disregarded, and the central particle is bound to move with the effective diffusion constant proposed by Honig et al.:[26]

$$D(d/a_i) = \frac{D_0}{\beta(d/a_i)} \quad (9)$$

where

$$\beta(d/a_i) = \frac{6[d/a_i]^2 + 13[d/a_i] + 2}{6[d/a_i]^2 + 4[d/a_i]} \quad (10)$$

As shown in ref 25, the present technique predicts a variation of the number of particles with time, which overlaps the results of eqs 6−7 in the absence of dense flocs, but also prevents overestimation of HI in concentrated systems.

Previous Results on the Dependence of k_f with ϕ. In a diffusion-controlled scheme of aggregation, the coagulation rate depends on the mean free path between particles. The average number of collisions is considered in eq 1 through the initial particle density (n_0), which neither accounts for the polydis-

persity of the initial particle size distribution (PSD), nor for hydrodynamic corrections of Stokes diffusion constant (eq 3).[27]

Hatton et al.[28] and Rarity et al.[29] studied the effect of the initial number of particles on the flocculation rate. Hatton et al. measured the flocculation rate of polystyrene latexes of 0.37 μm, 0.50 μm, 0.86 μm, and 1.9 μm in a 0.1 M solution of $MgSO_4$ using a flow ultra-microscope with laser illumination. k_f was found to increase from 2.6×10^{-18} m^3/s to more than 6.0×10^{-18} m^3/s when going from 10^{+6} to 10^{+10} particles per cm^3 (10^{+12} to 10^{+16} m^{-3}). These numbers correspond to changes in the volume fraction of the order of $10^{-8} < \phi < 10^{-4}$ for $a_i = 0.37$ μm and $10^{-6} < \phi < 10^{-2}$ for $a_i = 1.9$ μm. Rarity et al.[29] measurements also followed the concave increase of k_f vs n reported by Hatton et al. These authors further concluded that the rate constant at infinite dilution appeared to be only 50% of the theoretical value due to hydrodynamic effects between particles at close approach.

Recently, Hütter[27] studied the coagulation rate of Al_2O_3 particles in water ($2a_i = 0.5$ μm, $A = 4.76 \times 10^{-20}$ J, $0.20 < \phi \leq 0.40$) by means of BD without HI. To explain their results, this author noticed that the average time between collisions in diffusion-controlled aggregation should be roughly equal to $t = l^2/D_0$, where l is the mean surface-to-surface separation between two nearest neighbors in a randomly distributed configuration:

$$l = 2a_i\left[\sqrt[3]{\frac{\phi_m}{\phi}} - 1\right] \tag{11}$$

Here ϕ_m is the maximum volume fraction, which depends on the type of spatial arrangement of the particles. Accordingly, the time after which the number of particles has dropped to half its initial value ($t_{1/2}$) was supposed to be equal to

$$t_{1/2} = \alpha_1\left[\sqrt[3]{\frac{\phi_m}{\phi}} - 1\right]^{\alpha_2} \tag{12}$$

Parameters α_1 and α_2 were found to be to $\alpha_1 = 3.3 \times 10^{-2}$ s, $\alpha_2 = 2.23$, for that particular case, using $\phi_m = 0.479$ and a vanishing value of the surface potential.[27]

Although eq 12 is remarkably simple, it was used with success by Hütter to correlate flocculation data coming from BD simulations under a wide variety of conditions and repulsive barriers between the particles. Furthermore, it was recently used by our group[7] to study the dependence of $t_{1/2}$ with ϕ ($0.01 \leq \phi \leq 0.30$) for the case of 3.9-μm particles subject to thermal interaction only, or including an additional van der Waals attraction ($A = 1.24 \times 10^{-19}$ J). It was found that our BD data also followed eq 12 for the case of monodispersed systems, showing sizable deviations in the case of polydispersed ones. In that former case, it was encountered that $\alpha_1 = 140$ s, $\alpha_2 = 2.00$, and $\phi_m = 0.51$ (cubic packing).

As was shown in refs 7 and 25, BD simulations could be very helpful for the interpretation of experimental flocculation rates, since they allow the separate study of each contributing effect. In previous communications[7,25,30−33] we addressed the effects of polydispersity, thermal interaction, and surfactant adsorption on the flocculation rate in the absence of HI. Here, the effect of the volume fraction on k_f is studied in the case of a monodispersed distribution of particles of radius $a_i = 3.9$ μm, for two representative values of the Hamaker constant ($A = 1.24 \times 10^{-21}$ J, and $A = 1.24 \times 10^{-19}$ J) including HI. Furthermore, the application of eq 12 will be tested for this case, and the flocculation rates evaluated—whenever possible—by means of eq 1, and through the relation existing between $t_{1/2}$ and k_f ($t_{1/2} = 1/k_f n_0$).

It is important to remark that 3.9-μm particles are subject to a substantial gravitational force, which was purposely neglected, in the present calculations. The progressive incorporation of each contributing force will allow establishing their weight on the overall value of the flocculation rate. In the present case, gravitationally induced flocculation is not considered. It should be noticed that in this type of calculation the simulation box is very small with respect to the typical size of a macroscopic container. As a consequence, two-dimensional periodic boundary conditions (PBC) do not resemble the real situation, since no accumulation of particles should be observed as the result of gravitational effects on one extreme of the simulation box. Furthermore, three-dimensional PBC should not reproduce the behavior of the system at the bottom of the container, since the particle size distribution, which reaches a macroscopic volume of the emulsion from below, might be substantially different from the one leaving that volume from the opposite side.

Computational Details

In the original algorithm of Ermak and McCammon,[34] the position of a particle i at time $t + \Delta t$, depends on three terms: (1) the gradient of the diffusion tensor with respect to the particle's position, (2) a diffusive term given by the product of the diffusion tensor and the forces acting over the particle on each direction, and (3) a random contribution which summarizes the effect of the solvent molecules on the particle movement. As discussed in ref 25, the implementation of an average diffusion constant in Ermak and McCammon's algorithm[34] leads to a much simpler equation of motion, very similar to the one used in BD simulations in the absence of HI:[7,25,30−33]

$$r_i(t + \Delta t) = r_i(t) + \frac{D_i(\phi,d)F\Delta t}{kT} + R_G(D_i(\phi,d)) \tag{13}$$

Equation 13 corresponds to a forward-Euler integration of the equation of motion with a rate of convergence of first order. Here, $r_i(t)$ is the position of particle i at time t, and F is the sum of interparticle and external forces acting on i. $D(\phi,d)$ is the average diffusion constant of the particle which depends on its local volume fraction and the minimum distance of approach between particle "i" and its surrounding neighbors. The random function $R_G(D_i(\phi,d))$ is a Gaussian function with zero mean and variance $6D_i(\phi,d)\Delta t$.

In the present calculations, no repulsive forces are used. The particles aggregate *and coalesce* as the result of their Brownian motion and their van der Waals (vdW) attraction. According to Hamaker,[35] the attractive potential (V) between two drops of different sizes is equal to

$$V = -\frac{A}{12}\left[\frac{y}{x^2 + xy + x} + \frac{y}{x^2 + xy + x + y} + 2\ln\left(\frac{x^2 + xy + x}{x^2 + xy + x + y}\right)\right] \tag{14}$$

where A is the Hamaker constant, $x = d/2a_1$, $y = a_2/a_1$, a_k is the radius of particle k, and "d" is the shortest distance between the particles' surfaces.

It is important to notice that if the particles coalesce as soon as they touch, the distribution of particle sizes follows the prediction of eq 1, which was originally intended for the process of flocculation only.[30]

Except for the $\phi = 0.40$ case, all calculations started from a random distribution of 125 particles. Random spatial configurations are not possible at large volume fractions unless the particle

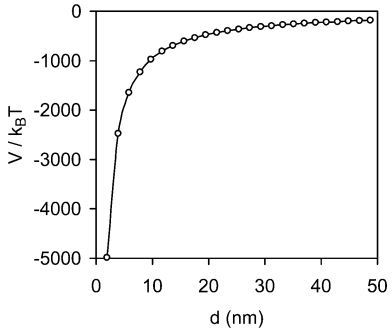

Figure 2. Variation of the van der Waals potential as a function of the distance of approach between two particles, for $A = 1.24 \times 10^{-19}$ J.

size distribution is polydisperse.[36−38] As shown in ref 7, the flocculation rate depends on the initial PSD, but the number of particles required in order to achieve volume fractions around 0.40 is too large for BD simulations. Consequently, a cubic arrangement was used for $\phi = 0.40$ and for a limited number of trial evaluations run at $\phi = 0.51$.

For the present purposes, cubic cells with 3-D periodic boundary conditions were employed. As explained in refs 30−32, we allow image-particles to coalesce with real particles in the same way they do with other real particles inside the simulation box. If the center of mass of the new particle fell outside the simulation box, its position corresponded to that of an image particle. In this case the new real particle was created applying periodic boundary conditions to the resulting coordinates.

The cutoff length of the potential was set equal to two particle radii (7.8×10^{-6} m), although the potential approaches negligible values at substantially smaller distances (Figure 2) $V(d = 7.8 \times 10^{-6}$ m, $A = 1.24 \times 10^{-19}$ J$) = -0.02\ kT$. The cell length was adjusted in each case to give the desired volume fraction, which was varied in the range $10^{-5} \leq \phi \leq 0.40$.

A double time-step scheme[25] was used in all simulations with $\phi < 0.10$. For this purpose, the maximum range of the interaction potential is used as input. A width of 50 nm was considered sufficient to capture the most relevant variation of the vdW potential appropriately (Figure 2). A double time-step calculation implies the use of a longer time step at long interparticle separation, and a short time step at distances lower than a pre-selected length $2L$ ($L = 50$ nm for this case). At each time step the program calculates the shortest distance between the particles. If this distance is smaller than $2L$, a short time step adequate for appropriate potential sampling is used (see below). Otherwise, the longer time step is employed.

Notice that the cutoff length of the potential is considerably longer than 50 nm. However, since the attractive potential does not change sharply with the distance for $d > 50$ nm, the potential can be sampled conveniently in this range using the longer time step.

For these calculations the small time step was set equal to 1.36×10^{-6} s ($= \Delta t_S$). It is known from previous calculations[7,25,30−33] that this time step is short enough to sample repulsive potentials 10-nm wide. The long time step (Δt_L) was set equal to 0.34 s, 5.44×10^{-2} s, 3.40×10^{-3} s, 3.40×10^{-5} s, 8.51×10^{-6} s, and 1.36×10^{-6} s, for volume fractions of 10^{-5}, 10^{-4}, 10^{-3}, $10^{-2} \leq \phi \leq 10^{-1}$, 0.20, and $0.30 \leq \phi \leq 0.40$, respectively. That is, $5.0 \times 10^{-9} \leq \Delta t_L^* \leq 1.25 \times 10^{-3}$ where $\Delta t_L^* = \Delta t_L D_0/a^2$, and $a = 3.9\ \mu$m.

Once the long and short time steps are selected, a double time-step calculation proceeds as follows. At the beginning of the simulation all particles move at Δt_L. The minimum separation between the particles is calculated at each iteration. If this distance is smaller than twice the pre-selected potential width, all particles are returned to their previous positions, and the shorter time step is used. Following, the particles move at this lower time step for $\Delta t_L/\Delta t_S$ iterations. When this inner cycle finishes, the particles had moved for a space of Δt_L seconds, going back in phase with the longer time step formerly used. The coalescence of droplets can only occur in the inner cycle, where the interacting potential is more finely sampled. The calculation proceeds in this way, entering the inner cycle from time to time whenever required.

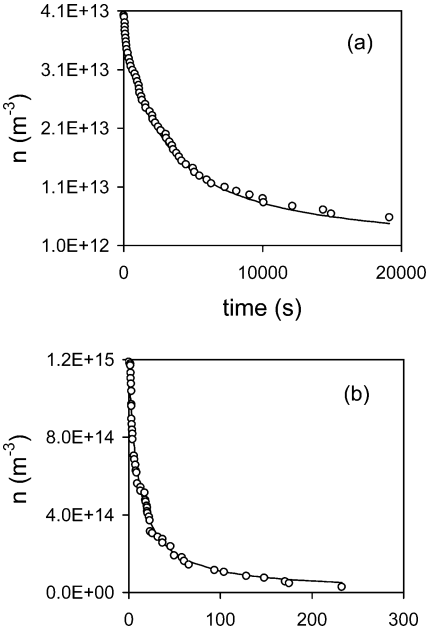

Figure 3. Change in the number of particles per unit volume n as a function of time, for (a) $\phi = 0.01$, and (b) $\phi = 0.30$, using $A = 1.24 \times 10^{-21}$ J. The simulation data is indicated by (o). Solid lines indicate the prediction of eq 1.

BD simulations were run either for 600 million iterations, or until the initial number of particles was reduced to only one particle, whichever happened first. One set of simulations corresponded to $A = 1.24 \times 10^{-21}$, and the other to $A = 1.24 \times 10^{-19}$. The flocculation constants were calculated in each case employing three different procedures: (1) through a plot of $1/n$ vs t, (2) through a plot of n vs t, minimizing the total difference between the values of $n(t)$ corresponding to the simulation and those calculated from eq 1 by varying the value of k_f, and (3) from the time required for the number of particles to drop to half their initial value $t_{1/2} = 1/k_f n_0$.

Results and Discussion

Figure 3 shows the variation of the number of particles per unit volume (n) as a function of time (t) for $\phi = 0.01$ (Figure 3a), and $\phi = 0.30$ (Figure 3b), using a Hamaker constant of $A = 1.24 \times 10^{-21}$ J. It can be observed that the BD data can be conveniently fitted to eq 1, represented in each picture by a continuous line. Typical regression coefficients of 0.9954 and 0.9864, respectively, were obtained for these two cases. Sizable deviations occur whenever the total number of particles decreases below ~20.

At higher volume fractions, the characteristic slope of eq 1 is lost and the data do not conform to Smoluchowski's predictions. This is illustrated in Figure 4a for $\phi = 0.40$ and $A = 1.24 \times 10^{-19}$ J. As discussed in ref 25, the strong

TABLE 1: Values of k_f and $t_{1/2}$ Obtained from the Simulations Using $A = 1.24 \times 10^{-21}$ J[a]

ϕ	k_f (m^3/s) (n vs t)	k_f (m^3/s) ($1/n$ vs t)	k_f (m^3/s) ($k_f = 1/t_{1/2}n_0$)	$t_{1/2}$ (s) (simulation)	$t_{1/2}$ (s) ($t_{1/2} = 1/k_f n_0$)
1.0×10^{-5}	6.70×10^{-18}	5.28×10^{-18}	6.78×10^{-18}	$3.66 \times 10^{+6}$	$4.70 \times 10^{+6}$
1.0×10^{-4}	6.25×10^{-18}	6.64×10^{-18}	6.93×10^{-18}	$3.61 \times 10^{+5}$	$3.76 \times 10^{+5}$
1.0×10^{-3}	7.70×10^{-18}	5.60×10^{-18}	8.08×10^{-18}	$3.07 \times 10^{+4}$	$4.43 \times 10^{+4}$
1.0×10^{-2}	9.68×10^{-18}	9.02×10^{-18}	9.01×10^{-18}	$2.75 \times 10^{+3}$	$2.75 \times 10^{+3}$
5.0×10^{-2}	9.94×10^{-18}	1.22×10^{-17}	1.04×10^{-17}	$4.77 \times 10^{+2}$	$4.09 \times 10^{+2}$
1.0×10^{-1}	1.22×10^{-17}	1.56×10^{-17}	1.17×10^{-17}	$2.12 \times 10^{+2}$	$1.59 \times 10^{+2}$
1.5×10^{-1}	2.52×10^{-17}	1.37×10^{-17}	1.96×10^{-17}	$8.44 \times 10^{+1}$	$8.84 \times 10^{+1}$
2.0×10^{-1}	2.61×10^{-17}	2.36×10^{-17}	2.80×10^{-17}	$4.44 \times 10^{+1}$	$5.26 \times 10^{+1}$
3.0×10^{-1}	8.24×10^{-17}	8.59×10^{-17}	9.32×10^{-17}	$9.02 \times 10^{+0}$	$9.79 \times 10^{+0}$
4.0×10^{-1}	1.12×10^{-16}	1.63×10^{-16}	7.86×10^{-17}	$7.90 \times 10^{+0}$	$3.80 \times 10^{+0}$

[a] The values of k_f shown in the second column were evaluated fitting the BD data to eq 1. Those of the third column correspond to the slope of $1/n$ vs t plots. Finally, the values of the fourth column were estimated using the relation $k_f = 1/n_0 t_{1/2}$, resulting from substitution of n by $n_0/2$ in eq 1. Column 5 shows the time required for the number of particles to drop to $n_0/2$ directly accessed from the simulations. These values can be also calculated using the flocculation constants of the third column ($t_{1/2} = 1/k_f n_0$).

TABLE 2: Values of k_f and $t_{1/2}$ Obtained from the Simulations Using $A = 1.24 \times 10^{-19}$ J[a]

ϕ	k_f (m^3/s) (n vs t)	k_f (m^3/s) ($1/n$ vs t)	k_f (m^3/s) ($k_f = 1/t_{1/2}n_0$)	$t_{1/2}$ (s) (simulation)	$t_{1/2}$ (s) ($t_{1/2} = 1/k_f n_0$)
1.0×10^{-5}	6.70×10^{-18}	7.11×10^{-18}	6.51×10^{-18}	$3.82 \times 10^{+6}$	$3.49 \times 10^{+6}$
1.0×10^{-4}	7.50×10^{-18}	8.93×10^{-18}	7.86×10^{-18}	$3.18 \times 10^{+5}$	$2.80 \times 10^{+5}$
1.0×10^{-3}	7.55×10^{-18}	7.71×10^{-18}	6.38×10^{-18}	$3.89 \times 10^{+4}$	$3.22 \times 10^{+4}$
1.0×10^{-2}	1.46×10^{-17}	1.41×10^{-17}	1.50×10^{-17}	$1.65 \times 10^{+3}$	$1.76 \times 10^{+3}$
5.0×10^{-2}	3.08×10^{-17}	2.36×10^{-17}	2.90×10^{-17}	$1.72 \times 10^{+2}$	$2.11 \times 10^{+2}$
1.0×10^{-1}	1.29×10^{-16}	5.49×10^{-17}	3.92×10^{-17}	$6.33 \times 10^{+1}$	$4.52 \times 10^{+1}$
1.5×10^{-1}	2.39×10^{-16}	1.37×10^{-16}	2.59×10^{-16}	$6.39 \times 10^{+0}$	$1.21 \times 10^{+1}$
2.0×10^{-1}	2.98×10^{-16}	1.64×10^{-16}	2.94×10^{-16}	$4.22 \times 10^{+0}$	$7.59 \times 10^{+0}$
3.0×10^{-1}	1.38×10^{-15}	9.22×10^{-16}	1.89×10^{-15}	4.40×10^{-1}	9.10×10^{-1}
4.0×10^{-1}	1.21×10^{-15}	4.32×10^{-15}	7.36×10^{-16}	8.40×10^{-1}	1.40×10^{-1}

[a] The origin of each entry is explained in the footnote of Table 1.

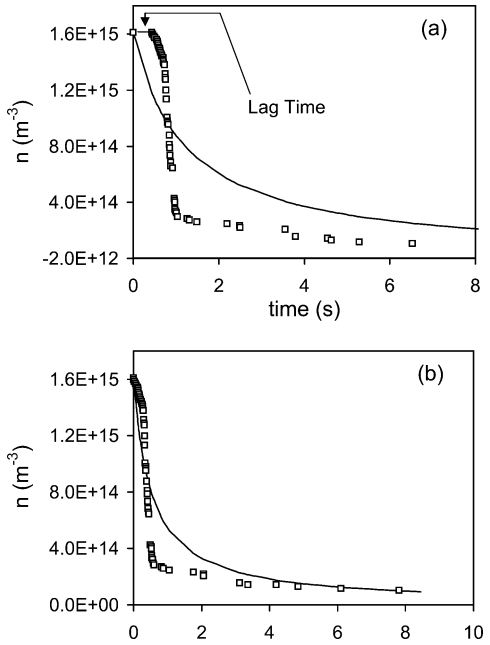

Figure 4. n vs t for $\phi = 0.40$ at $A = 1.24 \times 10^{-19}$ J. Squares (□) identify simulation data and solid lines the fitting of eq 1. (a) Total data set resulting from the simulation. (b) Suppression of the lag time favors the fitting of the flocculation (coalescence) rate.

hydrodynamic interaction between dispersed particles in concentrated systems generates a "lag time", that is, a finite period of time in which the drops move extremely slowly prior to the occurrence of the first coalescence. This lag time might be related to the decrease in the creaming velocity found in similar emulsions for $\phi \geq 0.40$.[39] Such a slow flocculation progressively concentrates the drops, generating a sharp decrease in the number of particles once the process of coalescence has begun. Elimination of the data corresponding to the referred lag time produces the curve shown in Figure 4b. This final curve can be better fitted to eq 1 in order to obtain a rough approximation to the flocculation rate at $\phi = 0.40$.

Values of the flocculation constant obtained from the previously outlined methodologies are shown in Tables 1 and 2 for $A = 1.24 \times 10^{-21}$ J and 1.24×10^{-19} J, respectively. Order of magnitude differences arise for volume fractions above 15% ($\phi > 0.15$). At lower volume fractions, the differences are sizable but considerably smaller.

The entries of Tables 1 and 2 corresponding to $\phi \leq 1 \times 10^{-3}$ also outline the limitations of the BD simulations for the calculation of flocculation rates. First, it should be noticed that not all simulation data are suitable for fitting. As discussed in ref 7, the simulations do not follow eq 1 once the number of particles decreases below 20−10 particles. Although we have carried out a limited number of 1000-particle simulations, it is computationally unfeasible to simulate a system of this size at $\phi \leq 1 \times 10^{-3}$, at least employing workstations. Thus, a considerable part of the data resulting from 125-particle simulations is lost for k_f evaluation purposes. Second, the long time step required for the BD simulation of very dilute systems may decrease artificially the number of collisions due to the considerable size of the random steps. Finally, due to the inherent characteristics of the data, different fitting procedures may produce reasonably large differences of k_f starting from the same simulation data (see Tables 1 and 2). As a general rule, estimations usually coincide whenever the simulation data can be fitted to eq 1 with a regression coefficient better than 0.98.

According to our simulations, HI improve the correlation coefficient in the absence of a repulsive barrier, since it diminishes the acceleration caused by van der Waals forces, and disfavors the occurrence of multiple collisions. In the

TABLE 3: Flocculation Rates and Regression Coefficients for a Selected Group of $\phi = 0.15$ Simulations in the Absence of Hydrodynamic Interactions

number of particles	driving force	particle size distribution	Hamaker constant	k_f (m^3/s)	regression coefficient
125	Brownian	monodisperse		6.00×10^{-17}	0.95011
1000	Brownian	monodisperse		4.80×10^{-17}	0.99421
125	Brownian	polydisperse		2.75×10^{-17}	0.98229
1000	Brownian	polydisperse		3.77×10^{-17}	0.99612
125	Vdw + Brownian	monodisperse	1.24×10^{-19}	1.70×10^{-16}	0.94683
1000	Vdw + Brownian	monodisperse	1.24×10^{-19}	1.40×10^{-16}	0.98871
125	Vdw + Brownian	polydisperse	1.24×10^{-19}	1.66×10^{-16}	0.97310
1000	Vdw + Brownian	polydisperse	1.24×10^{-19}	1.43×10^{-16}	0.97765

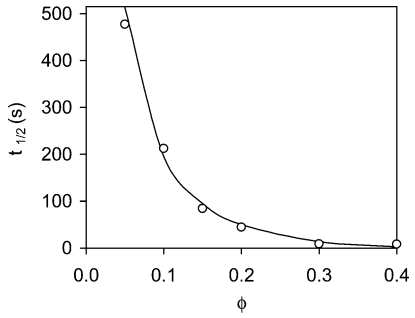

Figure 5. $t_{1/2}$ vs ϕ plot for Type I simulations ($A = 1.24 \times 10^{-21}$ J). The continuous line corresponds to the best fit of eq 12: $\alpha_1 = 375$ s, $\alpha_2 = 2.00$, and $\phi_m = 0.51$. The circles (o) show the results of the simulations.

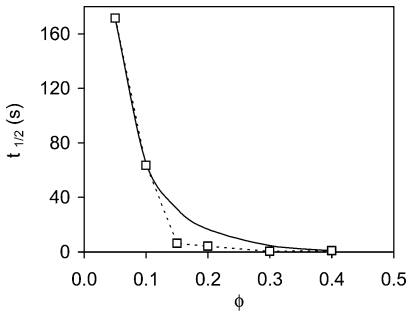

Figure 6. $t_{1/2}$ vs ϕ plot for Type II simulations ($A = 1.24 \times 10^{-19}$ J). The continuous line corresponds to the theoretical prediction given by eq 12 with $\alpha_1 = 125$ s, $\alpha_2 = 2.00$, and $\phi_m = 0.51$. The squares (□) illustrate the results of the simulations.

absence of HI and for a large value of the Hamaker constant ($A = 1.24 \times 10^{-19}$ J), the fitting of the simulation data to eq 1 shows regression coefficients appreciably smaller than those obtained in the present calculations. Those coefficients can be improved, increasing the number of particles in the simulation. Table 3 shows the results of 125-particle and 1000-particle calculations, for the specific case of $\phi = 0.15$ in the absence of hydrodynamic interactions. According to the limited amount of information currently available for 1000-particle simulations (Table 3), the flocculation constants calculated from 125-particle simulations may differ in approximately 1.5 units from those of 1000-particle simulations.

As a result of the above considerations, it is observed that the flocculation rate corresponding to $\phi = 1 \times 10^{-5}$ is higher than the one belonging to $\phi = 1 \times 10^{-4}$. A similar anomaly was also observed twice in Table 2 between $\phi = 1 \times 10^{-4}$ and $\phi = 1 \times 10^{-3}$. If an average deviation of the flocculation rate is calculated from the values forwarded by each methodology at $\phi = 1 \times 10^{-3}$, $\phi = 1 \times 10^{-4}$, and $\phi = 1 \times 10^{-5}$, a value of $\pm 1.34 \times 10^{-18}$ m^3/s results. This value is similar to the one obtained assuming that the flocculation rate is the same for $\phi \leq 1 \times 10^{-3}$, and computing the average deviation between all these values. The error comes out to be $\pm 1.37 \times 10^{-18}$ m^3/s. This is similar to the previous result and also to the magnitude error estimated in the previous paragraph.

Figure 5 shows that the $t_{1/2}$ data from the Type I simulations ($A = 1.24 \times 10^{-21}$ J) adjust very well to the predictions of eq 12. This is reasonable since there are no repulsive barriers between particles, and their motion is diffusive as assumed in the deduction of eq 1. This good behavior holds for $0.01 \leq \phi \leq 0.40$. As discussed by Hütter,[27] a characteristic linear growth of the mean square displacement with t implies $\alpha_2 = 2.0$. Furthermore, since ϕ_m corresponds to the maximum volume fraction, it can be either taken as 0.51 or 0.74, depending on the spatial configuration of the particle (cubic or hexagonal close-packed (HCP) arrangements, respectively). HCP calculations require special periodic boundary conditions which are difficult to implement in simulations with a variable particle size. With the usual cubic cells, the maximum packing fraction for monodispersed spheres corresponds to 0.52. Higher volume fractions can be achieved with a polydispersed particle size distribution, *if* the number of particles is increased considerably (> 500). Those calculations require a considerable computational effort. As shown by recent simulations on polydispersed systems,[7] polydispersity increases the standard deviation of the average flocculation rate at each volume fraction. For all these reasons, the highest volume fraction calculated in this work corresponds to $\phi = 0.51$. Thus, α_2 and ϕ_m were held constant at 2.0 and 0.51, respectively, while α_1 was varied in order to fit the data. The value of α_1 came out to be 375 s for Type I simulations and 125 s for Type II ($A = 1.24 \times 10^{-19}$) ones. As expected, the larger value of α_1 (larger $t_{1/2}$) corresponds to the weaker attractive force. Furthermore, the value of this parameter for Type II simulations is similar to the one formerly obtained under the action of the same attractive forces but in the absence of hydrodynamic corrections (140 s [7]). Unfortunately the fitting of the Type II data to eq 12 is less successful in this case than it was before (see Figures 5−6). This behavior is possibly related to the greater magnitude of the interaction potential for Type II simulations, since eq 12 only considers the diffusive behavior of the particles in the absence of interparticle forces. Since $t_{1/2}$ is also equal to the average time between collisions (see eq 1 and related discussion), it is clear that it is affected by the interaction potential in the vicinity of a collision, although it basically depends on the diffusive motion of the particles at longer distances.

As shown in Figure 6, considerable deviations of the data with respect to eq 12 are already observed for Type II simulations at a volume fraction of 0.01. Use of $t_{1/2}$ values calculated from $t_{1/2} = 1/k_f n_0$ does not improve this correlation significantly. However, it is important to notice that we are using only *one* initial configuration of the particles in order to predict the flocculation rate. The use of either a larger number of particles or an average $t_{1/2}$ value computed from a significant number of initial configurations will probably improve the fitting of the $t_{1/2}$ vs ϕ data to eq 12.

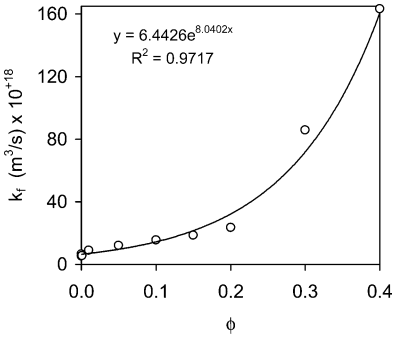

Figure 7. Variation of k_f as a function of the volume fraction (ϕ) for $A = 1.24 \times 10^{-21}$ J. The line correspond to an arbitrary exponential variation. The corresponding equation appears in the inset.

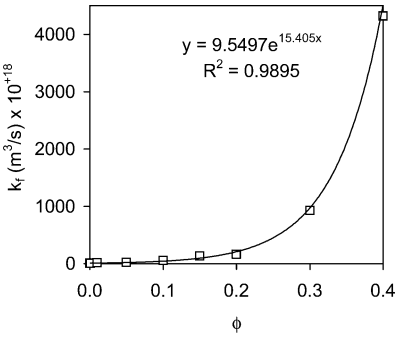

Figure 8. k_f vs ϕ for $A = 1.24 \times 10^{-19}$ J. The line corresponds to an arbitrary exponential equation given in the legend.

To provide a simple relationship between the flocculation constant and the volume fraction of the internal phase, the simulation data for each Hamaker constant was fitted to an exponential function (Figures 7 and 8). Exponential variations of the flocculation rate had been observed in bitumen emulsions subject to shearing,[40] and were used in the past with success to correlate similar simulation data.[30−32] Comparison of these two figures, as well as analysis of the numbers reported in Tables 1 and 2, clearly shows that k_f can reach values considerably larger than the one resulting from the random movement of the particles at infinite dilution: 5.49×10^{-18} m^3/s (eq 2). According to the exponential fittings, values of 6.44×10^{-18} m^3/s and 9.55×10^{-18} m^3/s are expected at very low concentrations for $A = 1.24 \times 10^{-21}$ J and $A = 1.24 \times 10^{-19}$ J, respectively. For these magnitudes of the attractive parameter A, a volume fraction increase from 10^{-5} to 0.40 raises the flocculation constant by more than 1 and 2 orders of magnitude, respectively.

As expected, the flocculation rates increase as the mean free path diminishes (eq 11). The mean free path is an important parameter in the evaluation of the flocculation rate since it summarizes the effects of polydispersity and volume fraction in only one variable. However, this variable is difficult to estimate for a random system. As shown in Figures 9 and 10, the values computed from eq 11 appear to be significant. The empirical curves shown in these figures provide an easy mean to estimate k_f as a function of the volume fraction for the set of Hamaker constants studied. These curves correspond to the equations $k_f = (45.5030\ l^{-2} - 1.6988\ l^{-1} + 7.2962) \times 10^{-18}$ m^3/s ($r^2 = 0.9897$) for $A = 1.24 \times 10^{-21}$ J, and $k_f = (631.10\ l^{-2} - 160.07\ l^{-1} + 18.159) \times 10^{-18}$ m^3/s ($r^2 = 0.9934$) for $A = 1.24 \times 10^{-19}$ J. Since the flocculation constant is inversely proportional to $t_{1/2}$, and $t \sim l^2/D_0$ in a diffusive regime, an approximately quadratic dependence between k_f and l^{-1} is not surprising.

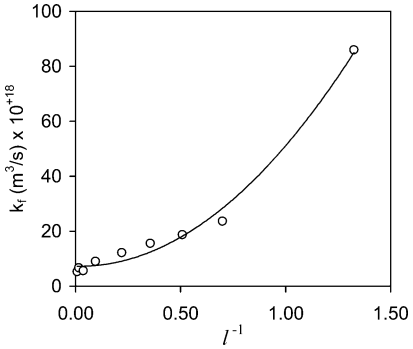

Figure 9. Increase of the flocculation rate with the decrease of the initial mean free path between drops (eq 11). $A = 1.24 \times 10^{-21}$ J. The line corresponds to a second-order polynomial fit.

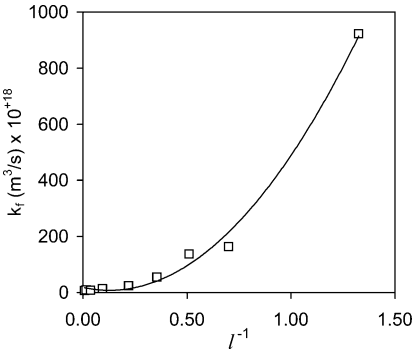

Figure 10. Increase of the flocculation rate with the decrease of the initial mean free path between drops (eq 11). $A = 1.24 \times 10^{-19}$ J. The line corresponds to a second-order polynomial fit.

Conclusions

Use of hydrodynamic corrections along with a double time-step technique allowed the calculation of flocculation rates by mean of Brownian dynamics simulations. The simulations provide reasonable estimates for k_f and $t_{1/2}$, allowing the establishment of empirical relations between these variables as a function of ϕ and l. The present methodology can be applied to either emulsions or dispersions. However, it must be kept in mind that the growth of aggregates in the latter case would conform to the evolution of their average hydrodynamic radii. In the present simulations, these radii increase as the result of the coalescence of particles, which is only possible if the particles are liquid.

According to these results, there is a pronounced dependence of k_f on ϕ. That dependence can be partially justified in terms of the initial mean free path of the particles in the dispersion. The rate of flocculation also depends on several other factors, such as the magnitude of the attractive force, the hydrodynamic interactions between particles, and the polydispersity of the system (which is unavoidable as the liquid/liquid dispersion evolves with time).

Finally, it was found that the increase of the Hamaker constant from 1.24×10^{-21} J to 1.24×10^{-19} J can change the flocculation rate in more than 1 order of magnitude depending on the volume fraction. Such changes can also represent large variations in the compositions of the particles. Thus, two dispersions with the same volume fraction may exhibit substantially different flocculation rates depending on the chemical nature of their internal phase.

The present simulations allow separating the contribution of the hydrodynamic interactions from that of the repulsive barriers in surfactant-stabilized systems. Commonly the stabilization factors of these systems are evaluated as the quotient between

the flocculation rate of the dispersion without surfactant and the one including the surfactant molecules. Comparison of the actual flocculation rates, k_f, with the present evaluations allows a more reliable estimation of the repulsive barrier in these systems. It should be noticed that the hydrodynamic interactions studied account for the movement of the intervening liquid between particles only. This is believed to be the most important type of hydrodynamic interaction in these systems. However, since the Stokes diffusion constant was assumed to be correct at infinite dilution, the variation of the friction, as a function of the nature of the particle/liquid interface, was not considered. An exact computation of stabilization factors requires the implementation of this additional hydrodynamic contribution. Unfortunately, such contributions depend on the chemical nature of the surfactant molecule.[13]

References and Notes

(1) von Smoluchowski, M. *Z. Phys. Chem.* **1917**, *92*, 129.

(2) Fuchs, N. A. *The Mechanics of Aerosols*; Dover Publications: New York, 1989; pp 288−352.

(3) Sonntag, H.; Strenge, K. *Coagulation kinetics and structure formation*; VEB Deutscher Verlag der Wissenschaften: Berlin, 1987; pp 14−178.

(4) Cohen, E. R.; Vaughan, E. U. *J. Colloid Interface Sci.* **1971**, *35*, 612.

(5) Lee, K. W. *J. Colloid Interface Sci.* **1983**, *92*, 315.

(6) Wang, C. S.; Friedlander, S. K. *J. Colloid Interface Sci.* **1967**, *24*, 170.

(7) Urbina-Villalba, G.; García-Sucre, M.; Toro-Mendoza, J. *Mol. Simul.* **2003**, *29*, 393.

(8) Verwey, E. J. W.; Overbeek, J. Th. G. *The Theory of Liophobic Colloids*; Dover: New York, 1999; pp 1−182.

(9) Fuchs, N. *Z. Physik* **1936**, *89*, 736.

(10) Holthoff, H.; Schmitt, A.; Fernández-Barbero, A.; Borkovec, M.; Cabrerízo-Vílchez, M. A.; Schurtenberger, P.; Hidalgo-Alvarez, R. *J. Colloid Interface. Sci.* **1997**, *192*, 463.

(11) Sonntag, H.; Shilov, V.; Gedan, H.; Lichtenfeld, H.; Dürr, C. *Colloids Surf., A* **1986**, *20*, 303.

(12) Dhont, J. K. G. *An Introduction to Dynamics of Colloids*; Elsevier Science B. V.: Amsterdam, 1996; Chapters 3 and 5.

(13) van de Ven, T. G. M. *Colloidal Hydrodynamics*; Academic Press Limited: Padstow, 1989; Chapters 1 and 2.

(14) Russel, W. B.; Saville, D. A.; Schowalter, W. R. *Colloidal Dispersions*; Cambridge University Press: Cambridge, 1989.

(15) Beenakker, C. W. J.; Mazur, P. *Phys. Lett. A* **1982**, *91*, 290.

(16) Beenakker, C. W. J.; Mazur, P. *Physica A* **1984**, *126*, 349.

(17) Rotne, J.; Prager, S. *J. Chem. Phys.* **1969**, *50*, 4831.

(18) Batchelor, G. K. *J. Fluid Mech.* **1982**, *119*, 379.

(19) Batchelor, G. K. *J. Fluid Mech.* **1976**, *74*, 1.

(20) Bacon, J.; Dickinson, E.; Parker, R. *Faraday Discuss.* **1983**, *76*, 165.

(21) Heyes, D. M. *Mol. Phys.* **1996**, *87*, 287.

(22) van Veluwen, A.; Lekkerkerker, H. N. W.; de Kruif, C. J.; Vrij, A. *Faraday Discuss.* **1987**, *83*, 59.

(23) van Megen, W.; Underwood, S. M.; Ottewill, R. H.; Williams, N. St. J.; Pusey, P. N. *Faraday Discuss.* **1987**, *83*, 47.

(24) Pusey, P. N.; van Megen, W. *J. Physique* **1983**, *44*, 285.

(25) Urbina-Villalba, G.; García-Sucre, M.; Toro-Mendoza, J. *Phys. Rev. E* **2003**, *68*, 061408.

(26) Honig, E. P.; Roebersen, G. J.; Wiersema, P. H. *J. Colloid Interface. Sci.* **1971**, *36*, 97.

(27) Hütter, M. *Phys. Chem. Chem. Phys.* **1999**, *1*, 4429.

(28) Hatton, W.; McFadyen, P.; Smith, A. L. *J. Chem. Soc., Faraday Trans.* **1974**, *70*, 655.

(29) Rarity, J. G.; Randle, K. J. *J. Chem. Soc., Faraday Trans.* **1985**, *81*, 285.

(30) Urbina-Villalba, G.; García-Sucre, M. *Langmuir* **2000**, *16*, 7975.

(31) Urbina-Villalba, G.; García-Sucre, M. *Interciencia* **2000**, *25*, 415.

(32) Urbina-Villalba, G.; García-Sucre, M. *Mol. Simul.* **2001**, *27*, 75.

(33) Urbina-Villalba, G.; García-Sucre, M. *Colloids Surf., A* **2001**, *190*, 111.

(34) Ermak, D.; McCammon, J. A. *J. Chem. Phys.* **1978**, *69*, 1352.

(35) Hamaker, H. C. *Physica (Amsterdam)* **1937**, *IV*, 1058.

(36) Sherwood, J. D. *J. Phys. A: Math. Gen.* **1997**, *30*, L832.

(37) Talbot, J.; Tarjus, G.; van Tassel, P. R.; Viot, P. *Colloids Surf., A* **2000**, *165*, 287.

(38) Torquato, S. *Phys. Rev. Lett.* **1995**, *74*, 2156.

(39) Chanamai, R.; McClemments, D. J. **2000**, *172*, 79.

(40) Cárdenas, A.; Rossi, S.; Pazos, D.; Rivas, H. *Visión Tecnológica* **1997**, *4*, 2.